Biochimica et Biophysica Acta 1788 (2009) 2204–2216

Contents lists available at ScienceDirect

Biochimica et Biophysica Acta

journal homepage: www.elsevier.com/locate/bbamem

A protective role for lipid raft cholesterol against amyloid-induced membrane damage in human neuroblastoma cells

Cristina Cecchi [a,b,*], Daniela Nichino [b,c], Mariagioia Zampagni [a], Caterina Bernacchioni [a], Elisa Evangelisti [a], Anna Pensalfini [a,1], Gianfranco Liguri [a,b], Alessandra Gliozzi [b,c], Massimo Stefani [a,b], Annalisa Relini [b,c]

[a] Department of Biochemical Sciences, University of Florence, Viale Morgagni 50, 50134 Florence, Italy
[b] Research Centre on the Molecular Basis of Neurodegeneration (CIMN), University of Florence, Italy
[c] Department of Physics, University of Genoa, Italy

ARTICLE INFO

Article history:
Received 25 March 2009
Received in revised form 16 July 2009
Accepted 23 July 2009
Available online 6 August 2009

Keywords:
ADDLs
Lipid raft cholesterol
ADDLs-GM1 colocalization
Amyloid-induced membrane damage
Alzheimer's disease

ABSTRACT

Increasing evidence supports the idea that the initial events of Aβ oligomerization and cytotoxicity in Alzheimer's disease involve the interaction of amyloid Aβ-derived diffusible ligands (ADDLs) with the cell membrane. This also indicates lipid rafts, ordered membrane microdomains enriched in cholesterol, sphingolipids and gangliosides, as likely primary interaction sites of ADDLs. To shed further light on the relation between ADDL–cell membrane interaction and oligomer cytotoxicity, we investigated the dependence of ADDLs binding to lipid rafts on membrane cholesterol content in human SH-SY5Y neuroblastoma cells. Confocal laser microscopy showed that Aβ1–42 oligomers markedly interact with membrane rafts and that a moderate enrichment of membrane cholesterol prevents their association with the monosialoganglioside GM1. Moreover, anisotropy fluorescence measurements of flotillin-1-positive rafts purified by sucrose density gradient suggested that the content of membrane cholesterol and membrane perturbation by ADDLs are inversely correlated. Finally, contact mode atomic force microscope images of lipid rafts in liquid showed that ADDLs induce changes in raft morphology with the appearance of large cavities whose size and depth were significantly reduced in similarly treated cholesterol-enriched rafts. Our data suggest that cholesterol reduces amyloid-induced membrane modifications at the lipid raft level by altering raft physicochemical features.

1. Introduction

Alzheimer's disease and other neurodegenerative disorders involve alteration of neuronal physiology, particularly at the synaptic level. Such alteration is thought to be mainly caused by Aβ1–40 and Aβ1–42 oligomers [1–3], which are also thought to cause cell impairment and death [4,5]. Mounting evidence supports the idea that the initial events of both Aβ oligomerization and oligomer cytotoxicity involve the interaction of the secreted Aβ peptides with the cell membrane [6–8]. However, in spite of the remarkable research efforts spent in the last years, the molecular basis of Aβ–membrane interaction and the ensuing structural modifications of the latter remains substantially elusive. Indeed, the question as to whether oligomer receptors or preferential interaction sites on the cell membrane do exist still awaits a convincing answer. The question is made even more intriguing by the increasing data indicating that amyloids grown from different peptides and proteins could behave similarly in their cytotoxic effects and, conversely, that structurally different amyloids grown under differing conditions from the same peptide/protein can display different cytotoxicities [9]. These evidences support the idea that amyloid cytotoxicity results from aggregate interaction with the cell membrane, with non-specific permeabilization of the latter [6,10–13].

A recent paper has shown that annular protofibrils grown from Aβ peptides are relatively stable and harmless to cultured neuronal cells and do not permeabilize synthetic lipid vesicles, contrary to similar protofibrils grown from prefibrillar oligomers at the lipid surface [14]. These data, together with immunological evidence, led the authors to

Abbreviations: Aβ, amyloid-β peptide; ADDLs, Aβ-derived diffusibile ligands; AFM, atomic force microscopy; AICD, Amyloid Precursor Protein Intracellular Domain; β-CD, methyl-β-cyclodextrin; BSA, bovine serum albumin; CR, Congo Red; ThT, thioflavin-T; CTX-B, cholera toxin subunit B; DAOS, N-ethyl-N-(2-hydroxy-3-sulfopropyl)-3,5-dimethoxyaniline; DMEM, Dulbecco's Modified Eagle's Medium; DMSO, dimethylsulfoxide; DPH, 1,6-diphenyl-1,3,5-hexatriene; DRMs, detergent-resistant membranes; EDTA, ethylenediaminetetraacetc acid; FBS, foetal bovine serum; GM1, monosialotetrahexosylganglioside; HEPES, N-2-hydroxyethylpiperazine-N-2-ethanesulfonic acid; HFIP, hexafluoro-2-isopropanol; HRP, horseradish peroxidase; Mev, mevastatin; PBS, phosphate buffered saline; PEG-cholesterol, polyoxyetanyl-cholesteryl sebacate; PMSF, phenylmethylsulfonylfluoride; WGA, wheat germ agglutinin

* Corresponding author. Department of Biochemical Sciences, University of Florence, Viale Morgagni 50, 50134 Florence, Italy. Tel.: +39 055 459 8320; fax: +39 055 459 8905.
E-mail address: cristina.cecchi@unifi.it (C. Cecchi).
[1] Present address: Department of Molecular Biology and Biochemistry, University of California, Irvine, CA 92697, USA.

0005-2736/$ – see front matter © 2009 Elsevier B.V. All rights reserved.
doi:10.1016/j.bbamem.2009.07.019

suggest that the toxic annular protofibrils may form pore structures into the membrane resembling those arising from pore-forming toxins. However, the studies on membrane permeabilization have been carried out mainly on synthetic lipid vesicles lacking the complex lipid and protein structure of the cell membrane. Therefore, any conclusion that amyloids are endowed by themselves with non-specific lipid membrane permeabilizing behaviour, although of value, cannot be directly extrapolated to cells, both in culture and in tissue, mainly as far as the specificity of the permeabilization effect is concerned.

The cell plasma membrane displays a complex structure with different regions coexisting in dynamic equilibrium. Among these, caveolae and lipid rafts – purified as detergent-resistant membrane fractions (DRMs) – appear to play key roles in many cellular processes, including endocytosis, signalling, oxidative stress, apoptosis, ion homeostasis and membrane protein trafficking and turnover [reviewed in 15,16]. DRMs are cholesterol-, sphingolipid- and ganglioside-rich ordered membrane microdomains freely floating through the more fluid lipid bilayer, which display very short half-lives and persistence times of the molecules embedded within them [17].

Lipid rafts contain a variable set of membrane proteins and their clustering is thought to provide a spatial and temporal meeting point for signalling molecules, as well as for molecules involved in processing and trafficking of membrane proteins. This includes the amyloid precursor protein (APP) and at least some of the proteases carrying on its cleavage [18–21]. In particular, lipid rafts have been proposed to function as platforms where neurotoxic oligomers of proteins and peptides, including the prion protein and the Aβ peptides, are assembled [22]. Actually, lipid rafts appear directly involved in prion protein stabilization and in the pathological conversion of the cellular (PrP^c) to the scrapie (PrP^{sc}) form [23,24]. Moreover, the PrP^c conformation can be stabilized upon association with lipid rafts in the secretory pathway [25]. Accordingly, it has been proposed that soluble Aβ peptide and prion protein aggregation can be raft-associated processes [26] and that any alteration of cholesterol (as well as sphingolipid) homeostasis can be a shared primary cause of a number of neurodegenerative diseases [27]. These findings, together with the presence, in the raft domains, of ligand-gated calcium channels (the AMPA and NMDA glutamate receptors) involved in Ca^{2+} influx into neuronal synaptic ends [28,29] and in Ca^{2+} permeabilization of amyloid-exposed cells [30,31] has implicated lipid rafts also in functional impairment of cells exposed to beta amyloid [32,33].

In spite of these and other recently reported data, no clear mechanistic evidence is presently available concerning the molecular and biochemical features of the relation between lipid rafts, their lipid content and dynamics, the generation of the aggregate precursors, as well as amyloid growth and toxicity. Recently, a study aimed at providing information on the proteins involved in extracellular Aβ internalization inside primary neuronal cells has suggested a caveolae-independent, raft-mediated mechanism. This implies lipid rafts as contributors not only to Aβ biogenesis and accumulation [34–36] but also to extracellular Aβ translocation [37] and aggregation [33]. Actually, it appears that APP fragments such as its intracellular domain (AICD) are able to interact with flotillin-1, a lipid raft marker protein, suggesting that it may recruit APP to lipid rafts favouring its localization and processing within these domains [38]. A recent report highlights a Fyn-dependent mechanism as a possible molecular basis of membrane-bound Aβ oligomer recruitment to lipid rafts [39].

Two alternative scenarios involving lipid rafts, based on conflicting experimental results have been proposed to describe the effect of cholesterol in Aβ generation and aggregation in AD. The high neuronal membrane cholesterol model for AD claims that high cholesterol favours APP processing with increased Aβ generation and aggregation through lipid raft clustering bringing into close contact the resident populations of APP and its processing enzyme β secretase-1 (BACE-1) [40]. The alternative low neuronal membrane cholesterol model claims that most of the APP is normally located in non-raft membrane domains. Accordingly, low membrane cholesterol would favour raft disassembly and BACE-1 translocation to non-raft domains supporting its contact with APP and enhancing cleavage of the latter with Aβ generation and aggregation [40]. Taken together, the findings reported in the last decade depict lipid rafts both as key domains where APP processing occurs and as primary interaction sites of ADDLs (and, possibly, other amyloid aggregates). However, much must still be learnt about the effective specificity and the biochemical, molecular and biological significance of such interaction.

To shed further light in the complex relation between the physicochemical features of lipid rafts and the ability of Aβ oligomers to interact with the cell membrane, we investigated the ability of ADDLs to bind raft-enriched membranes purified from normal human neuroblastoma cells or from the same cells enriched or depleted in cholesterol. The purified rafts were imaged by atomic force microscopy and their structural order was investigated by fluorescence anisotropy. We found that, in our model cells, any modification of the cholesterol content in the cell plasma membrane affects Aβ1–42 oligomer interaction with the latter. Our data agree with a number of previously reported findings indicating that increased cholesterol content in the plasma membrane reduces membrane disassembly by Aβ oligomers and protects against its cytotoxicity [7,41].

2. Materials and methods

2.1. Materials

All reagents were of analytical grade or the highest purity available. Foetal bovine serum (FBS), phosphate buffered saline (PBS), hexafluoro-2-isopropanol (HFIP), polyoxyetanyl-cholesteryl sebacate (PEG-cholesterol), methyl-β-cyclodextrin (β-CD), mevastatin (Mev), filipin III and other chemicals were from Sigma (Milan, Italy) unless otherwise stated. Wheat germ agglutinin (WGA)-conjugated fluorescein and Alexa Fluor 647-conjugated cholera toxin subunit B (CTX-B) were from Molecular Probes (Eugene, OR). Aβ1–42 and reversed Aβ42–1 peptides, as trifluoroacetate salts, were from Bachem (Bübendorf, Switzerland). Aβ1–42 amine-reactive succinimidyl esters of carboxyfluorescein (Aβ42-FAM) were from AnaSpec (San Jose, CA). Aβ peptides were dissolved in HFIP at 1.0 mM concentration and incubated for 1.0 h at room temperature to allow complete peptide monomerization [42]. Then, aliquots of peptide solutions were dried under nitrogen and stored at −80 °C. Aggregate concentrations were those of the monomeric Aβ1–42 peptide.

2.2. Cell culture and membrane cholesterol modulation

Human SH-SY5Y neuroblastoma cells were obtained from A.T.C.C. (Manassas, VA) and cultured in DMEM/F-12 Ham with 25 mM HEPES and $NaHCO_3$ (1:1) supplemented with 10% FBS, 1.0% glutamine and 1.0% antibiotics. Cell cultures were maintained in a 5.0% CO_2 humidified atmosphere at 37 °C and grown until 80% confluence. Cells were used for a maximum of 20 passages. The increase of the membrane cholesterol content was achieved by supplementing the cell culture media with 0.1 mM PEG-cholesterol for 1.0 h at 37 °C, as previously described [7]. Membrane cholesterol depletion was achieved by incubating the cells with 1.0 mM β-CD for 30 min at 37 °C in serum-free medium or with 10 μM Mev for 48 h at 37 °C in the presence of 1.0% FBS. The amount of cholesterol in membrane fractions and in purified rafts was assayed by the Amplex Red Cholesterol Assay Kit (Molecular Probes, Eugene, OR) [43]. Sample cholesterol was oxidized by 1.0 U/ml cholesterol oxidase for 30 min at 37 °C to yield H_2O_2 and the corresponding ketone product. In the presence of 1.0 U/ml horseradish peroxidase (HRP), H_2O_2 reacted with 150 μM 10-acetyl-3,7-dihydroxyphenoxazine (Amplex Red reagent) with a 1:1 stoichiometry to generate the highly fluorescent resorufin [44]. At the end of the incubation, sample fluorescence was

measured at 544 nm excitation and at 590 nm emission. Cholesterol content was determined by comparison with a reference curve built by assaying various cholesterol amounts (in the 50–1000 ng range). The amount of sphingomyelin in rafts purified from SH-SY5Y cells was assayed by a photometric method with the Sphingomyelin Assay Kit (Cayman Chemical, Ann Arbor, MI). Briefly, sample sphingomyelin was hydrolyzed by sphingomyelinase to phosphorylcholine and ceramide for 60 min at 37 °C. The choline resulting from the subsequent incubation of phosphorylcholine with alkaline phosphatase was oxidized by choline oxidase with production of H_2O_2. The latter was reacted in the presence of peroxidase with N-ethyl-N-(2-hydroxy-3-sulfopropyl)-3,5-dimethoxyaniline (DAOS) and 4-aminoantipyrine, yielding a blue color product with an optimal absorption at 595 nm [45]. Sphingomyelin was quantified by comparison with a reference curve built by assaying known amounts of sphingomyelin (in the 25–800 ng range).

2.3. Prefibrillar Aβ aggregate preparation and treatment

Prefibrillar aggregates of the Aβ1–42 peptide processed as reported above were obtained according to the Lambert's protocol [42]. Briefly, aliquots of Aβ1–42 were dissolved in DMSO to a final concentration of 5.0 mM, incubated in ice-cold F12 medium to 100 μM at 4 °C for 24 h and then centrifuged at 14,000×*g* for 10 min. The supernatant, defined as the amyloid β-derived diffusible ligand (ADDL) preparation, consisted of a fibril-free solution of globular assemblies 1.5 nm high, as assessed by tapping mode AFM (Fig. 7B+, inset). Taking into account a height correction factor of about 2.5 for sample drying under mild vacuum [46], a globule height of about 4.0 nm was calculated. This value agrees with the ADDLs height previously measured by AFM [46]. When needed, the cell cultures were pretreated with 1.0 μM (final concentration) ADDLs. The same concentration was used to treat isolated raft fractions for fluorescence anisotropy measurements and AFM analysis. In another set of experiments, the cells were treated with 3.0 μM fluorescein-labeled Aβ42-FAM aggregates containing a mixture of Aβ42-FAM peptide with 2 molar equivalents of unlabeled Aβ1–42 peptide (at a 1:2 ratio) to minimize possible interference of the fluorophore with the aggregation, while retaining sufficient fluorescence signal [47].

2.4. Confocal analysis

Labelling of membrane cholesterol was achieved by the fluorescent probe filipin III. Briefly, the cells seeded on glass coverslips were fixed in 4.0% buffered paraformaldehyde for 20 min at 0 °C and then incubated with 0.25 mg/ml filipin III in PBS for 24 h at 37 °C. After washing, the cells were fixed again in 4.0% buffered paraformaldehyde for 20 min at 0 °C prior to confocal scanning microscope analysis. Aβ1–42 aggregate binding to the plasma membranes was monitored in neuroblastoma cells seeded on glass coverslips by confocal scanning microscopy, as previously described [7]. Briefly, cells exposed for 30 min to 1.0 μM ADDLs were counterstained with fluorescein-conjugated WGA (5 μg/ml) for 10 min to detect the plasma membrane profiles. After washing, the coverslips were incubated with mouse monoclonal anti-Aβ antibodies 6E10 (Signet, DBA, Italy) and diluted 1:1000 in PBS with 1.0% FBS for 60 min. The immunoreaction was revealed by incubation for 90 min with Texas Red-conjugated anti-mouse secondary antibodies (Vector Laboratories, DBA, Italy), diluted 1:1000 in PBS containing 1.0% FBS. Negative controls were obtained by substituting the blocking solution for the primary antibody. Aggregate–cell interactions were also analyzed by treating cells with 3.0 μM Aβ42-FAM oligomers and counterstaining the plasma membranes with Alexa Fluor 633-conjugated WGA, but without fixing cells in buffered paraformaldehyde, without permeabilizing the plasma membrane and without using antibodies. Aβ1–42 aggregate colocalization with the cell surface lipid raft GM1 marker was monitored in SH-SY5Y neuroblastoma cells seeded on glass coverslips by confocal scanning microscopy. After treatment with 1.0 μM Aβ1–42 aggregates for 30 min, the cells were fixed in 2.0% buffered paraformaldehyde for 10 min at room temperature. After washing, the coverslips were incubated with mouse monoclonal anti-Aβ antibodies 6E10 and with 1:1000 diluted fluorescein-conjugated anti-mouse secondary antibodies (Vector Laboratories, DBA, Italy). Then, the cell surface GM1 was counterstained with 10.0 μg/ml CTX-B in cell culture media for 20 min at room temperature. Cell fluorescence was analyzed by a confocal Leica TCS SP5 scanning microscope (Mannheim, Germany) equipped with an argon laser source for fluorescence measurements using excitation lines at 488 nm, 510 nm, 568 nm, 633 nm and 647 nm for fluorescein, filipin III, Texas Red, Alexa Fluor 633-conjugated WGA and Alexa Fluor 647-conjugated CTX-B, respectively. A series of optical sections (1024×1024 pixels) 1.0 μm in thickness was taken through the cell depth for each examined sample and projected as a single composite image by superimposition. To quantify the fluorescence intensity of filipin III, a variable number of cells ranging from 10 to 22 were analyzed in each experiment. Fluorescence signals are expressed as fractional changes above the resting baseline, $\Delta F/F$, where F is the average baseline fluorescence in control cells (assumed as 100%) and ΔF represents the fluorescence changes over the baseline. GM1 colocalization with Aβ1–42 aggregates on the cell membrane was estimated on regions of interest (12–13 cells) using the ImageJ (NIH, Bethesda, MD, USA) and JACOP plugin (rsb.info.nih.gov) softwares [48].

2.5. Aβ aggregate binding to the cell membrane

Aggregate adsorption to the cell surface was analyzed as previously described [7]. Briefly, 5.0×10^3 cells/well, exposed for 1.0 h to 0.1 mM PEG-cholesterol or to vehicle, were treated with 1.0 μM Aβ1–42 aggregates for 0 or 30 min in a 96-well plate and then washed twice with PBS. The residual aggregate–cell complex was stained with 100 μl of 1.0 μM Congo Red (CR) in PBS for 20 min and measured photometrically at 490 nm (free CR) and 550 nm (bound CR) with an ELISA plate reader. CR values were reported as percent increases in treated cells *versus* untreated cells (taken as 100%).

2.6. Amyloid cytotoxicity assay

The effect of ADDLs on neuroblastoma cell morphology was investigated by Hoechst 33342 dye staining. Briefly, after exposure to 1.0 μM Aβ1–42 aggregates for 24 h at 37 °C, the cells were incubated with 20 μg/ml Hoechst for 15 min at 37 °C and fixed as reported above. Blue fluorescence micrographs of cells were obtained under UV illumination in an epifluorescence inverted microscope (Nikon, Diaphot TMD-EF) with an appropriate filter set. Aggregate cytotoxicity to neuroblastoma cells was assessed in 96 well plates by the MTT assay as previously reported [7]. Briefly, after exposure to 1.0 μM Aβ1–42 aggregates for 24 h at 37 °C, the cell cultures were incubated with a 0.5 mg/ml MTT solution at 37 °C for 4.0 h and then with cell lysis buffer (20% SDS, 50% N,N-dimethylformamide, pH 4.7) overnight. The absorbance values of blue formazan were determined at 590 nm. Cell viability was expressed as percent of MTT reduction in treated cells as compared to cognate untreated cells, where it was assumed as 100%. Finally, lactate dehydrogenase (LDH) release into the culture media, a typical necrotic marker, was measured after cell exposure to 1.0 μM Aβ1–42 aggregates for 48 h at 37 °C by the LDH assay kit (Roche Diagnostics, Mannheim, Germany) at 490 nm after blank subtraction at 595 nm.

2.7. Membrane and lipid raft purification

Total cell lysates were obtained from neuroblastoma cells by three freeze–thaw cycles followed by 5.0 s ultrasonication in ice in 20 mM Tris–HCl buffer, pH 8.0, containing 1.0% Triton X100, 137 mM NaCl,

10% glycerol, 6.0 M urea, 0.1 mM PMSF, 10 μg/ml leupeptin, 10 μg/ml aprotinin and by centrifugation at 14,000×*g* for 10 min at 4 °C. Membrane fractions were obtained as previously described, with minor modifications [7]. Briefly, the cells were homogenized in PBS containing 9.0% sucrose with three freeze–thaw cycles, 5.0 s sonication in ice and centrifugation at 700×*g* for 10 min at 4.0 °C. The membrane fraction was pelleted by a further supernatant centrifugation at 110,000×*g* for 1.0 h at 4.0 °C. Protein content in the cell lysates and in the membrane fractions was measured by the method of Bradford [49]. Lipid raft and non-raft fractions were prepared as described in Romiti et al. [50]. Briefly, the culture media of control, PEG-cholesterol-, β-CD-, or Mev-treated SH-SY5Y cells was removed and the cells were washed twice with ice-cold PBS, scraped, and collected by centrifugation at 1000×*g*. Then, the cells were dispersed in a 10 mM Tris–HCl buffer, pH 7.5, containing 150 mM NaCl, 5.0 mM EDTA, 1.0 mM Na_3VO_4, 1.0% Triton X-100 (TNE buffer) and protease inhibitors (10 μg/ml leupeptin and 10 μg/ml aprotinin). After a 20 min incubation in ice, the cells were disrupted in a Dounce homogenizer (80 strokes) and centrifuged at 1500×*g* for 5.0 min at 4.0 °C to obtain the post-nuclear fraction. The latter was adjusted to 40% (w/v) sucrose by 1:1 addition of 80% sucrose prepared in TNE buffer, placed at the bottom of an ultracentrifuge tube and overlaid with two layers of 30% and 5.0% sucrose in TNE buffer. The gradient was then centrifuged at 170,000×*g* for 18 h at 4.0 °C using a Beckman SW50 rotor. The resulting gradient was analyzed by collecting 0.4 ml fractions from the top of the gradient. Immunoblot analysis was performed to assess the fractions containing raft microdomains. Representative amounts of each fraction from the sucrose gradient were run on 12% (w/v) SDS/PAGE and the separated proteins blotted onto a PVDF Immobilio-P Transfer Membrane (Millipore Corporation, Bedford, MA). The blotted membranes were blocked in 1.0% (w/v) BSA in TBS-Tween (0.1 % Tween 20 in 20 mM Tris–HCl buffer, pH 7.5, containing 100 mM NaCl) and then incubated with mouse anti-flotillin-1 monoclonal antibodies (BD Biosciences, San Diego, CA). After extensive washing, the membranes were incubated with peroxidase-conjugated anti-mouse secondary antibodies (Pierce, Rockford, IL, USA) for 1.0 h and the immunolabelled bands were detected using a SuperSignal West Dura (Pierce, Rockford, IL, USA). The flotillin-1-positive fractions were pooled and extensively dialysed against TNE buffer to remove sucrose.

2.8. Steady-state fluorescence anisotropy

Fluorescence anisotropy (r) of 1,6-diphenyl-1,3,5-hexatriene (DPH) (Sigma Milan, Italy) was used to measure the structural order of the hydrophobic region of the purified DRMs under steady-state conditions. Anisotropy measurements were performed at 37 °C by a Perkin-Elmer LS 55 luminescence spectrometer equipped with manual polarizers. Excitation and emission wavelengths were set at 360 nm and 425 nm, with a slit-width of 2.5 nm and 4 nm, respectively. Our system was initially calibrated using DPH in mineral oil, which is expected to give an anisotropy value of 1.0. The *g* factor was calculated using horizontally polarized excitation and subsequent comparison of the horizontal and vertical emissions. The DRMs were incubated for 0, 1, 10, 30 and 60 min in the presence of either Aβ1–42 aggregates or the Aβ42–1 reverse peptide, and then further incubated for 30 min with DPH at a 1:250 probe-to-lipid ratio. Fluorescence intensity was measured with the excitation polarizer in the vertical position and the analyzing emission polarizer in both the vertical (I_{VV}) and the horizontal (I_{VH}) positions. The anisotropy constant, *r*, was calculated using the equation:

$$r = \frac{I_{VV} - gI_{VH}}{I_{VV} + 2gI_{VH}}$$

DRM fluorescence intensity in the absence of DPH was measured to evaluate the effect of light scattering.

2.9. Atomic force microscopy (AFM)

AFM analysis was carried out on 50 μl aliquots of the purified DRMs deposited on freshly cleaved mica, incubated for 1.0 h and then rinsed with Milli-Q water. AFM measurements were performed using a Dimension 3100 scanning probe microscope (Digital Instruments, Veeco, Santa Barbara, CA) equipped with a Nanoscope IIIa controller and a "G" scanning head (maximum scan size 100×100 μm). Tapping mode AFM would be expected to minimize lateral forces and allow better imaging of soft samples. Raft membranes were an exception, as we could not image them in tapping mode, even using different cantilevers and solution conditions. It is possible that when operating in tapping mode an oscillation is also induced in the sample. This would explain why tapping mode imaging of DRMs was impossible. On the other hand, when operating in contact mode, a force is steadily applied to the sample, resulting in an improved stability of the system. Thus images were acquired in contact mode in liquid by using V-shaped non-conductive silicon nitride cantilevers (type DNP, Veeco; 115 μm length, nominal spring constant 0.58 N/m) with pyramidal tips (nominal curvature radius in the 20–60 nm range) and scan rate in the 0.5–2.0 Hz range. Images were captured as 512×512 pixel images. The minimum force employed in contact mode imaging was 0.3 nN.

The morphological features of the samples were analyzed in terms of height and width in cross section in the topographic AFM images. The heights of the steps associated either to membrane domains or to cavities were measured with respect to the background. The sizes of each domain (or hollow) were the mean of the widths measured along the major diameter of the domain (or hollow) and the corresponding in-plane perpendicular direction. Due to tip size effects, which cause an apparent increase of the size of the imaged object in the image plane, domain sizes are overestimated respect to the real ones. To evaluate the expected widths, *w* (reported in Table 1), we modelled the domain as a flat object with half-spherical edges, using the equation:

$$w = w_{app} + 2h - 2\sqrt{2hR_T + h^2}$$

where w_{app} and *h* are the measured width and height, respectively, and R_T is the AFM tip radius.

We used a silicon calibration grating with ultrasharp tips (NT-MDT TGT01, Silicon-MDT Ltd., Moscow, Russia) to measure the curvature radius R_T for four tips of the same type and we obtained a mean value of 25 ± 7 nm. This value, which is within the range provided by the manufacturer, has been used to evaluate the correction for tip enlargement effects, according to the procedure quoted above.

The possible changes in raft morphology induced by the interaction with Aβ1–42 oligomers were investigated in samples prepared as described above incubated for 30 min in the presence of 1.0 μM ADDLs, rinsed with Milli-Q and imaged in liquid.

Table 1
Interaction with ADDLs affects the morphological features of DRMs.

Raft samples	Pore depth (nm)	Pore size (nm)	Domain size (nm)	Domain height (nm)
Control			455 ± 15	1.68 ± 0.04
Control + Aβ1–42	1.50 ± 0.04	420 ± 20	218 ± 12	0.68 ± 0.02
Chol-enriched			356 ± 16	1.78 ± 0.03
Chol-enriched + Aβ1–42	1.03 ± 0.03	370 ± 30	332 ± 18	0.81 ± 0.04
Chol-depleted			540 ± 40	1.17 ± 0.06
Chol-depleted + Aβ1–42	1.30 ± 0.03	450 ± 30	261 ± 11	1.22 ± 0.04
Aβ1–42 treated cells	0.68 ± 0.04	120 ± 10	470 ± 40	0.83 ± 0.03

Each pore (or domain) size figure was the mean of the widths measured along the pore (or domain) major diameter and the corresponding in-plane perpendicular direction. Domain heights were measured with respect to the image background. The data are expressed as mean ± standard error over an ensemble of at least 100 measurements.

To check the presence of the GM1 ganglioside, after deposition on the mica substrate the DRMs were incubated for 30 min with rabbit polyclonal anti-GM1 antibodies (Calbiochem; EMD Chemicals Inc., Darmstadt, Germany), diluted 1:1000. The presence of flotillin-1 in the samples deposited on the mica substrate was assessed by incubating the rafts with 0.5 μg/ml mouse anti-flotillin-1 antibodies (BD Transduction Laboratories; BD Biosciences, USA) for 30 min.

The domains imaged in the DRMs samples were better characterized by incubation with a mixture of carboxypeptidase Y from baker's yeast, thermolysin from *Bacillus thermoproteolyticus rokko* Type X and α-chymotrypsin from bovine pancreas Type VII (Sigma; Milan, Italy), at final concentrations of 1.0 mg/ml, 5.0 mg/ml and 5.0 mg/ml, respectively. Protease digestion was carried out by incubating the rafts with the protease mixture for 2.0 h either before or after sample deposition on the mica substrate.

To characterize morphologically the Aβ1–42 aggregates, 20 μl aliquots of ADDLs, obtained as reported above, were deposited on freshly cleaved mica substrates and dried under mild vacuum. The images were acquired in tapping mode in air using a Dimension 3100 AFM microscope (as detailed above) and a Multimode scanning probe microscope equipped with an "E" scanning head (maximum scan size 10 μm). Single beam uncoated silicon cantilevers (type OMCL-AC, Olympus, Japan) were used. The drive frequency was around 300 kHz and the scan rate was in the 0.3–0.8 Hz range.

2.10. Statistical analysis

Except the AFM data, all other data are expressed as mean ± standard deviation (SD). Comparisons between the different groups were performed by ANOVA followed by Bonferroni's *t*-test. A p value <0.05 was considered statistically significant. AFM data concerning sample morphological features are expressed as mean ± standard error over an ensemble of at least 100 measurements. All the statistical analyses had a confidence level ≥95%.

3. Results

3.1. Aβ1–42 oligomer binding to the cell surface and its cytotoxic effect are modulated by membrane cholesterol content

In previous studies we showed that the interaction of amyloid aggregates of different peptides and proteins with the plasma membranes of several types of cultured cells is significantly inversely correlated to the membrane content of cholesterol [7,51,52]. Here, we modulated the cholesterol content in human neuroblastoma cells by incubating the cells in the presence of PEG-cholesterol, β-CD or Mev. Cell treatment with PEG-cholesterol significantly increased the content of cholesterol in the cell membrane (13.55 ± 0.68 μg/mg protein, $p \leq 0.05$) *versus* control cells (10.84 ± 0.54 μg/mg protein) as assayed by the Amplex Red Cholesterol Assay Kit. Conversely, membrane cholesterol content was significantly reduced by cell treatment with β-CD (7.26 ± 0.73 μg/mg protein, $p \leq 0.05$) and Mev (9.71 ± 0.46 μg/mg protein, $p \leq 0.05$) *versus* control cells. These data were confirmed by confocal analysis of the sensitive fluorescent probe filipin III (Fig. 1A). Then, we evaluated the ability of our ADDLs to bind to the plasma membrane of neuroblastoma cells after a 30 min period of exposure by qualitative confocal microscope analysis of anti-Aβ1–42 antibody fluorescence (Fig. 1B). In addition, photometric quantitative measurement of specific Congo Red signal showed that, in cells supplemented with PEG-cholesterol, the increase of plasma membrane cholesterol resulted in a reduced Aβ1–42 oligomer binding to the plasma membrane (plus 113% CR signal *vs* untreated cells), as compared to control cells (plus 142% *vs* untreated cells). Conversely, the same oligomers added to the cell culture medium accumulated to a greater extent at the plasma membrane of cells with low membrane cholesterol content (plus 155% *vs* untreated cells). To exclude any possible interference of the cell fixation favouring the intracellular uptake of ADDLs, the distribution of fluorescein-labeled Aβ42-FAM aggregates was analyzed in unfixed neuroblastoma cells. Green fluorescence signal confirmed the different membrane distribution of ADDLs at our experimental conditions (Fig. 1B).

We also evaluated whether an increased content of membrane cholesterol was able to prevent amyloid toxicity at our experimental conditions. As shown in Fig. 1C, the quantitative analysis of the ability of the treated cells to reduce MTT and the morphological evaluation of Hoechst 33342 stained cells revealed no marked characteristics of apoptosis in cells enriched in cholesterol after their exposure to ADDLs for 24 h. On the other hand, the loss of membrane cholesterol in cells treated with β-CD or Mev before exposure to the aggregates resulted in a marked increase in the number of cells displaying nuclear condensation and a significant impairment of viability respect to similarly exposed cells with basal cholesterol content. Finally, we investigated whether neuroblastoma cells exposed to ADDLs for 48 h underwent a necrotic cell death. As shown in Fig. 1C, a significant release of LDH in the cell culture media was observed in cells with basal and, to a greater extent, reduced cholesterol content exposed to ADDLs. Also in this case, cholesterol-enriched cells displayed a higher resistance to amyloid toxicity, as compared to control cells, as revealed by the significant reduction of LDH release in the culture media.

3.2. Aβ1–42 oligomers colocalize with lipid rafts

Cholesterol is not uniformly distributed into the plasma membrane. In fact, it is concentrated into the outer leaflet, particularly in lipid rafts. The latter appear to exist in a liquid-ordered phase contributing to their partitioning from the surrounding liquid-disordered glycerophospholipid-rich environment. Lipid rafts are considered primary interaction sites of ADDLs [39]. Therefore, we sought to assess whether the modified ability of our ADDLs to interact with normal, cholesterol-enriched or depleted cells implied the participation of lipid rafts. Confocal laser microscopy showed a marked colocalization of Aβ1–42 oligomers with GM1, a well known lipid raft marker, on the plasma membranes of our neuroblastoma cells (Fig. 2). In particular, when the images were merged, a number of yellow areas representing the colocalization of membrane-bound ADDL with GM1 were seen. The scatter plots of fluorescence signals over the highlighted areas are shown in Fig. 2 (right). Two different algorithms, the Pearson's correlation coefficient and the overlap coefficient according to Manders gave similar results. In particular, the analysis over three different experiments yielded a colocalization of 43% between GM1 and ADDLs in control cells. Interestingly, a moderate enrichment of membrane cholesterol in PEG-chol treated cells appeared to reduce the ADDLs interaction with the monosialoganglioside GM1 as supported by the low degree of colocalization (19%) , while an increased colocalization was found in β-CD (69%) and Mev (67%) treated cells.

Overall, our colocalization data show that Aβ oligomers interact with the plasma membrane preferentially at the raft domains and that any structural modification of the latter following increase or decrease of cell cholesterol results in alterations of ADDL–raft interaction. These findings agree with previously reported data, showing that the content of cholesterol in cell membranes or in synthetic lipid vesicles modulates membrane–aggregate interaction [7,41], pointing at the membrane rafts as the key sites where those modifications do occur.

3.3. Isolation and characterization of DRMs

After having analyzed the ADDL–raft interaction in normal, cholesterol-enriched, or depleted SH-SY5Y cells, we investigated by confocal microscopy the modification of lipid raft morphology and distribution in the plasma membranes of cells enriched or depleted in

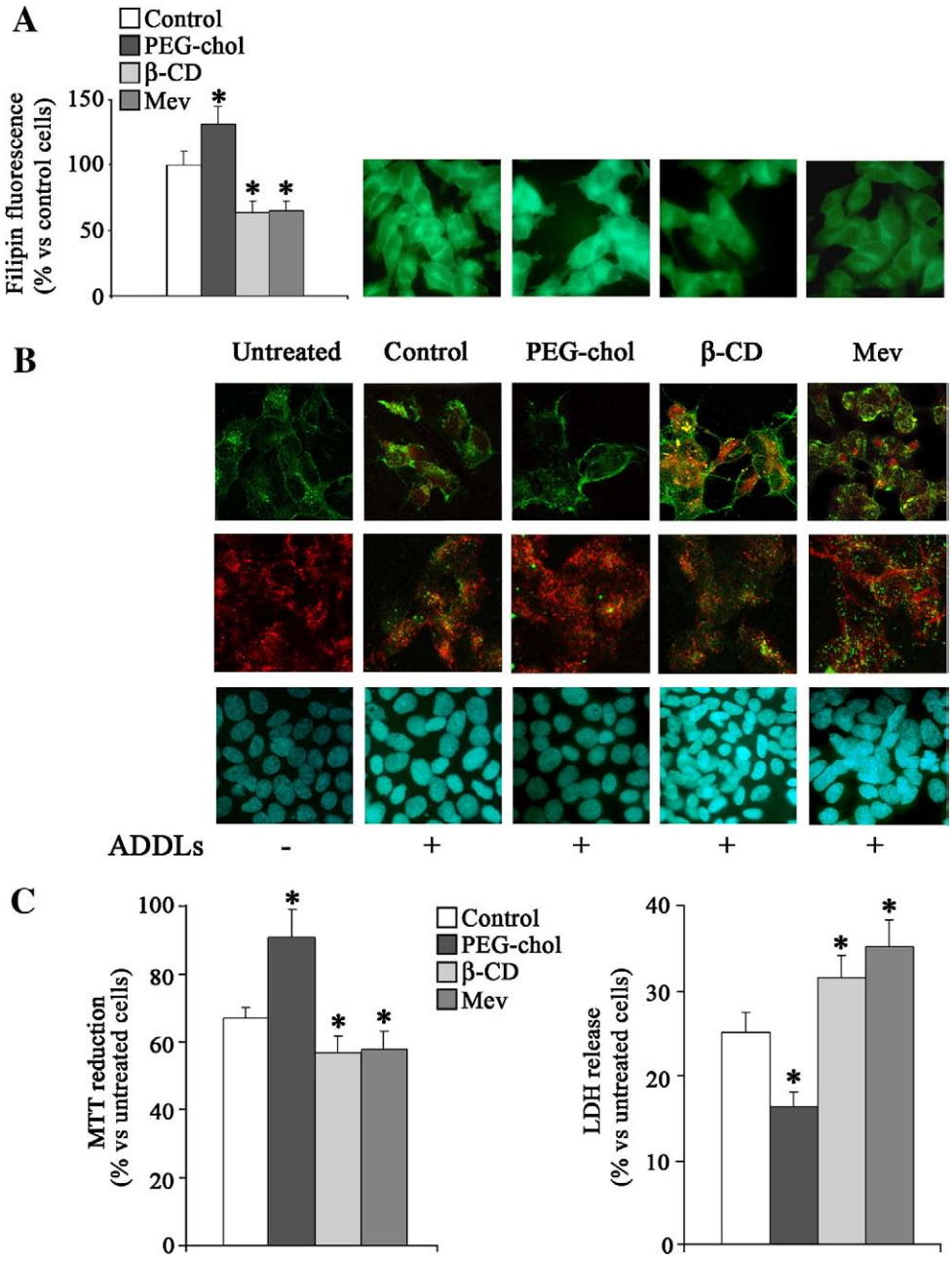

Fig. 1. (A) Representative confocal microscope analysis of membrane cholesterol content in SH-SY5Y neuroblastoma cells probed by the fluorescent dye filipin III (for details, see under Materials and methods). Neuroblastoma cells were analyzed at basal conditions (Control), 1.0 h after incubation with 0.1 mM PEG-cholesterol (PEG-chol), 30 min after cell culture supplementation with 1.0 mM β-methylcyclodextrin (β-CD) and 48 h after incubation with 10 μM mevastatin (Mev). Filipin III fluorescence is expressed as fractional change above the resting baseline, $\Delta F/F$, where F is the average baseline fluorescence in control cells (assumed as 100%) and ΔF represents the fluorescence changes over the baseline. The values shown are means ± S.D. of three independent experiments each carried out in triplicate. $^{*}p \leq 0.05$, significant difference *vs* control cells. (B) Representative confocal microscope images showing aggregates penetrating into the plasma membrane of neuroblastoma cells treated with 1.0 μM Aβ1–42 ADDLs (top) or with 3.0 μM Aβ42-FAM aggregates (middle) for 30 min. Representative blue fluorescence micrographs of Hoechst 33342 stained cells, after exposure to 1.0 μM ADDLs for 24 h (bottom). Untreated cells (−) are compared with cells exposed to amyloid oligomers at basal conditions, after treatment with PEG-chol, β-CD and Mev, respectively (+). The first set of images (top) was acquired on fixed cells, counterstaining with fluorescein-conjugated WGA to detect the plasma membrane profile (green), while Aβ1–42 aggregates were labelled with monoclonal mouse 6E10 anti-Aβ antibodies and Texas Red-conjugated anti-mouse secondary antibodies (red). The second set of images (middle) was obtained by analyzing unfixed cells treated with Aβ42-FAM oligomers (green) by counterstaining the plasma membranes with Alexa Fluor 633-conjugated WGA (red). (C) Membrane cholesterol enrichment by PEG-cholesterol treatment significantly protects neuroblastoma cells against amyloid aggregate toxicity as assessed by the 3-(4,5-dimethylthiazol-2-yl)-2,5-diphenyltetrazolium bromide (MTT) reduction test. The reported values are representative of four independent experiments, each performed in triplicate. Cell viability was checked by LDH release into the culture medium after exposure to 1.0 μM Aβ1–42 aggregates for 48 h. The values shown are means ± S.D. of three independent experiments, each performed in triplicate. $^{*}p \leq 0.05$, significant difference *vs* control cells.

cholesterol by labelling the cell surface GM1. GM1-positive membrane domains did not appear uniformly distributed on the plasma membranes and some more brightly stained domains were observed in control cells (Fig. 3). PEG-cholesterol treatment apparently increased the brightness of GM1-rich domains, without any evident alteration of their surface distribution. On the other hand, a substantially reduced CTX-B fluorescence was evident in cholesterol-depleted cells, confirming that the content of membrane cholesterol is crucial for lipid raft organization, possibly by regulating in a dose-dependent manner both their formation and function.

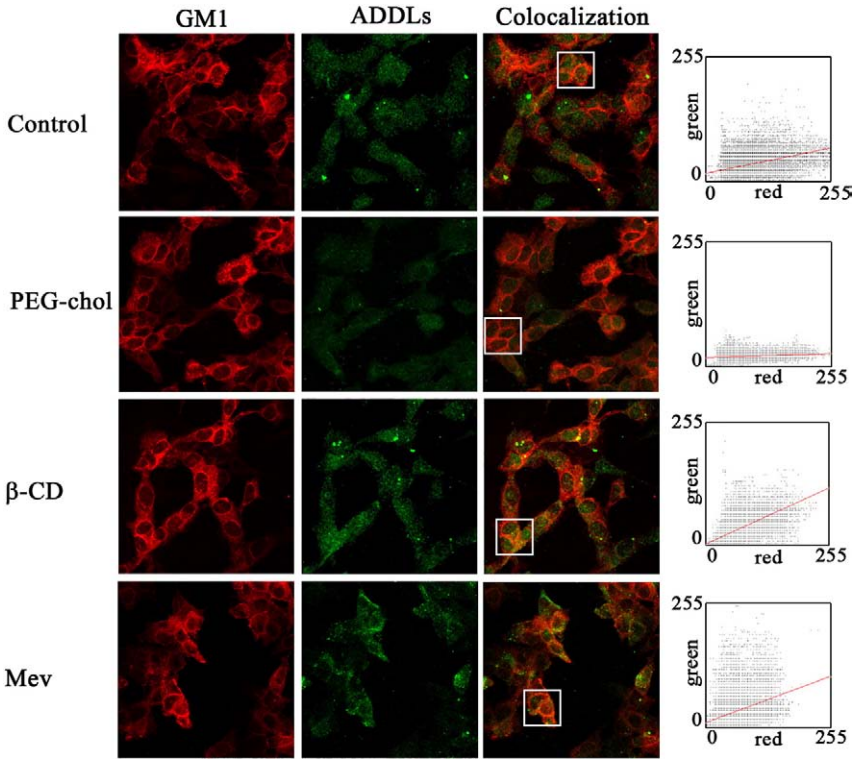

Fig. 2. Representative confocal microscope images showing ADDL colocalization with GM1 (yellow), a typical marker of lipid rafts in neuroblastoma cells. Top, control cells; second row, PEG-chol treated cells; third and fourth row, β-CD and Mev-treated cells, respectively. Aβ1–42 oligomers were labelled with monoclonal mouse 6E10 anti-Aβ antibodies and fluorescein-conjugated anti-mouse secondary antibodies (green), while GM1 was stained with fluorescent CTX-B conjugate as a probe (red). The GM1-ADDL colocalization on the cell membranes was estimated. The scatter plots indicate the colocalization pattern over the selected area of each panel; the sampled pixels were plotted as a function of red (*x* axis) and green (*y* axis) fluorescence intensity, resulting in a partial (top), low (second row) or high (third and fourth row) GM1-ADDL colocalization.

Next, we investigated the effects of the same treatments directly on lipid raft fractions isolated from treated or control neuroblastoma cells. Due to their insolubility in non-ionic detergents at low temperatures, lipid rafts have been defined as detergent-resistant membranes (DRMs). Because of their high lipid-to-protein ratio, DRMs display a low density and can be isolated by cell lysis with Triton X-100 and flotation on sucrose density gradients. Sucrose gradient fractions, purified from human neuroblastoma cells untreated or treated with PEG-cholesterol or with β-CD or Mev, were analyzed by Western blot for the presence of flotillin-1, a lipid raft protein marker. As shown in Fig. 3, flotillin-1 was localized in low density fractions (2–5) in control cells. In agreement with confocal analysis, cholesterol enrichment did not affect remarkably the DRM density distribution. On the contrary, in β-CD and Mev-treated cells most of the flotillin-1 immunoreactivity was shifted to fractions 12–14. However, a minor flotillin-1 immunoreactivity was still present in fractions 2–5, suggesting that β-CD or Mev treatment led to a partial, not complete, disruption of the organization and/or the number of lipid rafts in our cell model.

After extensive dialysis to remove sucrose, the amount of cholesterol was quantified in the pooled flotillin-1-positive fractions (2–5) purified from cells enriched or depleted in cholesterol or from control cells. As expected, the amount of cholesterol in the plasma membrane microdomains was significantly increased (+20% *vs* control cells) or reduced (−40% *vs* control cells) upon cell treatment with PEG-cholesterol or with β-CD and Mev, respectively (Fig. 3). No significant difference was observed in the total sphingomyelin levels among DRMs pools obtained from control cells (2.17 ± 0.32 ng/μl), cholesterol-enriched cells (2.09 ± 0.23 ng/μl) and cholesterol-depleted cells (1.94 ± 0.45 ng/μl).

3.4. Effects of ADDLs on lipid raft structural order

The effect of cholesterol on membrane fluidity is known to be complex; cholesterol can either enhance or decrease membrane fluidity depending on temperature, cholesterol concentration and bilayer composition [53]. However, under physiological conditions cholesterol is known to increase membrane rigidity. Thus, we evaluated the effect of cholesterol content on the structural order of the hydrophobic regions of lipid rafts by measuring the fluorescence anisotropy of 1,6-diphenyl-1,3,5-hexatriene (DPH) under steady-state conditions at 37 °C. The relative motion of the DPH dye molecule within the fatty acid acyl chain space of the lipid bilayer was determined by polarized fluorescence and expressed as *r*, the anisotropy constant, whose value is inversely proportional to the degree of membrane fluidity [54,55]. As expected, in raft-enriched samples prepared from neuroblastoma cells a moderate cholesterol enrichment significantly increased the raft structural order, whereas cholesterol depletion resulted in a higher fluidity (Fig. 4).

We also investigated whether the content of cholesterol in lipid rafts modified the membrane perturbing effect of ADDLs. We found a rapid reduction of fluidity in control lipid rafts exposed to 1.0 μM Aβ1–42 oligomers for various lengths of time (Fig. 4, *inset*). As the most ordered structure was reached in less than 10 min of exposure to the oligomers, we chose this incubation time for subsequent experiments. No evident difference in DPH fluorescence anisotropy was detected by exposing lipid rafts to Aβ42–1, suggesting that this effect is specific of the β-sheet structure found in ADDLs. Cholesterol-enriched lipid rafts did not display any significant change of the anisotropy upon exposure to Aβ1–42 oligomers or to the reverse Aβ42–1 peptide, suggesting that cholesterol enrichment protects lipid rafts from perturbation by Aβ1–42. On the contrary, cholesterol loss resulted in

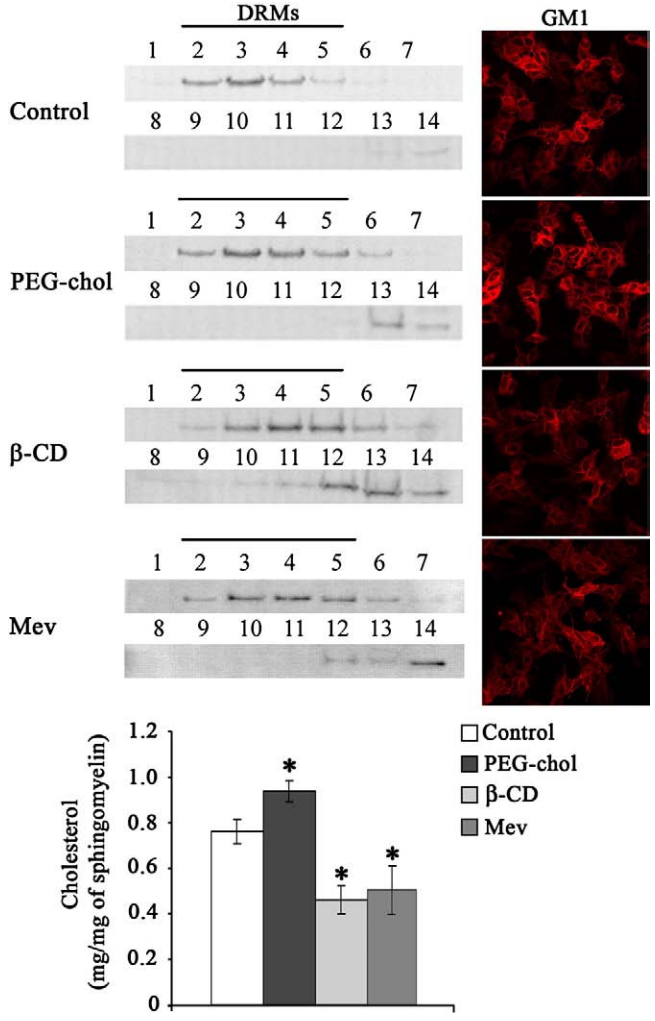

Fig. 3. A, representative immunoblot analysis of flotillin-1 levels in 14 sucrose gradient fractions collected from the top (low density) through the bottom (high density) of the gradient tube, as described under Materials and methods. An aliquot from each fraction was run on 12% SDS/PAGE, transferred onto a PVDF membrane and then incubated with mouse anti-flotillin-1 monoclonal antibodies. Flotillin-1-positive fractions enriched in lipid raft microdomains (from 2 to 5) were pooled and extensively dialyzed against TNE buffer to remove sucrose. Then the amount of cholesterol in the DRM pools was determined by a fluorimetric assay and expressed as ratio to sphingomyelin content. The reported values are means ± S.D. of four independent experiments, each performed in duplicate. $^{*}p \leq 0.05$, significant difference *vs* control cells. On the right side of the figure, representative confocal analysis of the cell surface GM1 distribution in SH-SY5Y neuroblastoma cells probed by the fluorescent CTX-B conjugate (for details, see under Materials and methods). Neuroblastoma cells were analyzed at basal conditions (Control), 1.0 h after incubation with 0.1 mM PEG-cholesterol (PEG-chol), 30 min after cell culture supplementation with 1.0 mM β-methylcyclodextrin (β-CD) and 48 h after cell incubation with 10 μM mevastatin (Mev).

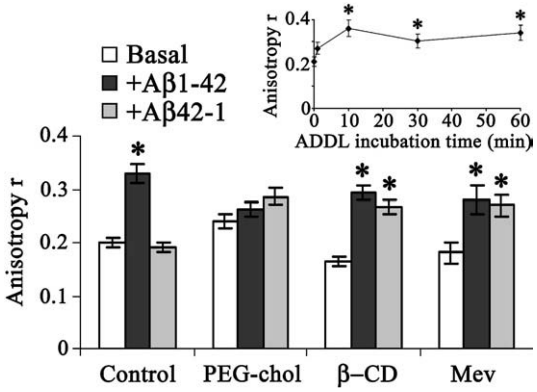

Fig. 4. DPH fluorescence anisotropy, *r*, measured before and after DRM treatment with Aβ1–42 ADDLs or the Aβ42–1 peptide. The measurements were performed on control, cholesterol-enriched and cholesterol-depleted samples. A moderate increase of the content of cholesterol in DRMs purified from PEG-cholesterol (PEG-chol)-treated cells enhanced DPH anisotropy when compared to DRMs prepared from control cells, whereas a decrease in the anisotropy was seen in DRMs prepared from cells depleted in cholesterol upon treatment with β-CD or Mev. Addition of Aβ1–42 oligomers induced a significant decrease of the fluidity of DRMs prepared from control or cholesterol-depleted cells, while the reverse Aβ42–1 peptide affected only cholesterol-poor microdomains. (*inset*) DPH fluorescence anisotropy, *r*, measured by incubating rafts for 2, 10, 30 and 60 min in the presence of 1.0 μM Aβ1–42 oligomers. All the data are means ± S.D. of six independent experiments, each performed in duplicate. $^{*}p \leq 0.05$, significant difference *vs* untreated microdomain fluidity.

increased rigidity of rafts exposed not only to Aβ1–42 ADDLs, as expected, but also to Aβ42–1 monomers, suggesting that the latter are able to penetrate and stiffen the raft bilayer as well, although with reduced efficiency.

3.5. AFM imaging of supported DRMs purified from cells exposed to ADDLs

The deposition of purified DRMs on mica substrates for AFM inspection resulted in the spontaneous formation of membrane multilayers, similarly to the behaviour observed when supported bilayers are formed from liposome deposition [56,57]. The DRM multilayers completely covered the imaging field and there was no mica substrate exposed. However they did not appear homogeneous, with membrane domains sprouting from a uniform background (Fig. 5A). The background thickness with respect to the mica surface, measured by indenting the background in different points, corresponded to up to four double layers (each about 5 nm thick). The domains were stable upon scanning (Fig. 5B) and had a typical lateral size of a few hundred of nm. Their height with respect to the background was less than 2 nm (Table 1). To check whether the sprouting domains had the same chemical nature of the background, we performed antibody labelling experiments to detect the presence of GM1 and flotillin-1, typical components of membrane rafts. Fig. 5D shows a representative image obtained in the presence of anti-GM1 antibodies. A uniform distribution of granular structures located in the background is observed, indicating the presence of GM1 in this region. As the DRM multilayers completely covered the imaging field, we can rule out the possibility of any non-specific interaction of anti-GM1 antibodies with the mica. No granular structures were observed on the domain surface, although incubation with anti-GM1 antibodies resulted in domain fragmentation. A similar behaviour was observed with anti-flotillin-1 antibodies (data not shown). AFM force–distance measurements (not shown) indicated that the adhesion forces measured on the domains are much stronger than those on the background, indicating that the domains are more fluid than the background [58].

To check whether proteins were the main component of these domains, we incubated the DRMs with a cocktail of proteases, as described under Materials and methods. DRM treatment with the proteases before deposition on the mica substrate resulted in the disappearance of membrane domains and the presence of a homogeneous sample surface (data not shown). Conversely, when DRMs were incubated with proteases after deposition on the mica substrate, the domains originally present were very unstable upon scanning (Fig. 6A, B) and disappeared after a few scans. As mentioned above, successive scans performed in the absence of proteases (Fig. 5A, B) showed that the domains can be reproducibly imaged and therefore their instability observed in the presence of proteases can actually result from the action of the latter. These results suggest that the background is composed by DRMs, while the slightly higher domains are formed by fluid phase-separated proteins or lipid–protein complexes present in the DRM preparations.

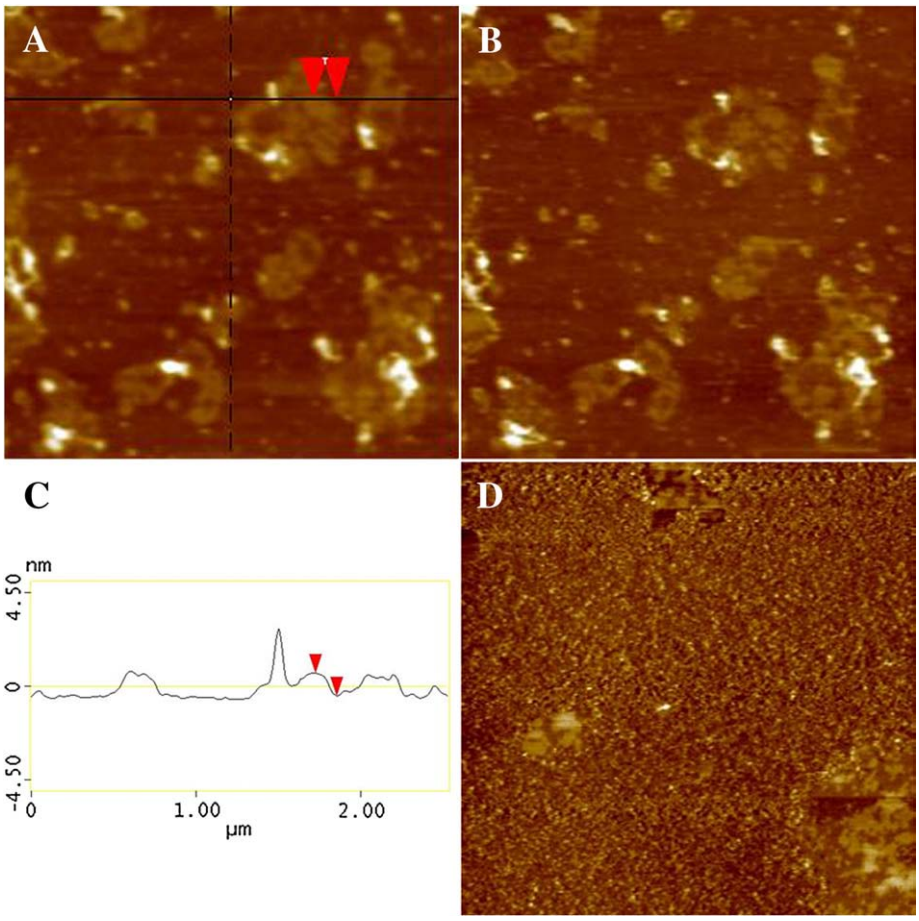

Fig. 5. (A) Contact mode AFM image in liquid (height data) of DRMs extracted from control cells; (B) a subsequent scan of the same area showing reproducibility of domain imaging. The image in (B) was taken 15 min after that in (A); (C) height profile obtained from an image section along the horizontal line indicated in (A); (D) imaging of DRMs labeled with anti-GM1 antibodies. Scan size 2.5 µm; Z range (A, B) 10 nm, (D) 5 nm.

DRMs purified from cholesterol-enriched and cholesterol-depleted cells were also imaged by AFM. In samples purified from cholesterol-enriched cells the lateral size of the membrane domains appeared reduced as compared with that measured in control samples which, in turn, was reduced with respect to that measured in DRMs purified from cholesterol-depleted cells (Table 1). This finding could be explained by the effect of cholesterol on membrane fluidity, resulting in decreased mobility, and therefore reduced coalescence, of fluid domains, in agreement with the fluorescence anisotropy data reported above.

Next, we investigated the effect of cell exposure to ADDLs on DRM morphology. DRMs purified from cells treated with Aβ1–42 oligomers before raft extraction (Fig. 6C) displayed the presence of cavities, or hollows (white arrows), whose depth and size are reported in Table 1. Corral-like structures (1.7 ± 0.1) nm high and (260 ± 10) nm in diameter were also observed (Fig. 6C). Both cavities and corral-like structures were absent in DRMs purified from cells treated with Aβ42–1 oligomers before raft extraction (Fig. 6D), suggesting a non generic interaction of Aβ1–42 with lipid rafts. Fig. 7 compares the morphologies of DRMs extracted from control (Fig. 7A), cholesterol-enriched (Fig. 7B) and cholesterol-depleted (Fig. 7C) cells before (−) and after (+) exposure to ADDLs. The latter are imaged in the inset in Fig. 7B. The presence of the peptide clearly altered DRM morphology, giving rise to the formation of cavities in all samples. The quantitative analysis of the images showed that the depth and size of the cavities observed in cholesterol-enriched samples were significantly reduced with respect to those displayed by cholesterol-depleted samples. All DRMs treated with Aβ1–42 oligomers after purification displayed cavities with depths and sizes significantly increased as compared to those found in DRMs purified from cells previously exposed to the same oligomers. In particular, a four-fold increase in the cavity sizes was observed (Table 1). These results indicate that a reduced raft damage was caused by ADDLs in living cells with respect to that found in purified DRMs.

In addition to cavity formation, DRM exposure to ADDLs resulted in changes of domain morphology. In fact, exposure of DRMs purified from control and cholesterol-enriched cells to ADDLs resulted in a remarkable reduction of domain heights (as measured with respect to the image background) to values similar to those observed in DRMs purified from cells previously exposed to Aβ oligomers. On the contrary, domain height was substantially unchanged in DRMs purified from cholesterol-depleted cells (Table 1).

The domain lateral size in DRM preparations from control and cholesterol-depleted cells exposed to Aβ oligomers was reduced, while that of DRMs from cholesterol-enriched cells was substantially unchanged, suggesting that cholesterol hinders the ADDL-DRM (and possibly raft) interaction. Furthermore, the domain size in DRMs purified from cells treated with Aβ1–42 oligomers was the same as that of the DRMs purified from control, not exposed, cells suggesting a possible recovery of the membrane structure *in vivo*.

4. Discussion

In the present study we investigated whether membrane cholesterol can influence ADDL cytotoxicity to human neurotypic SH-SY5Y cells by modulating either the physical state of the cell membrane,

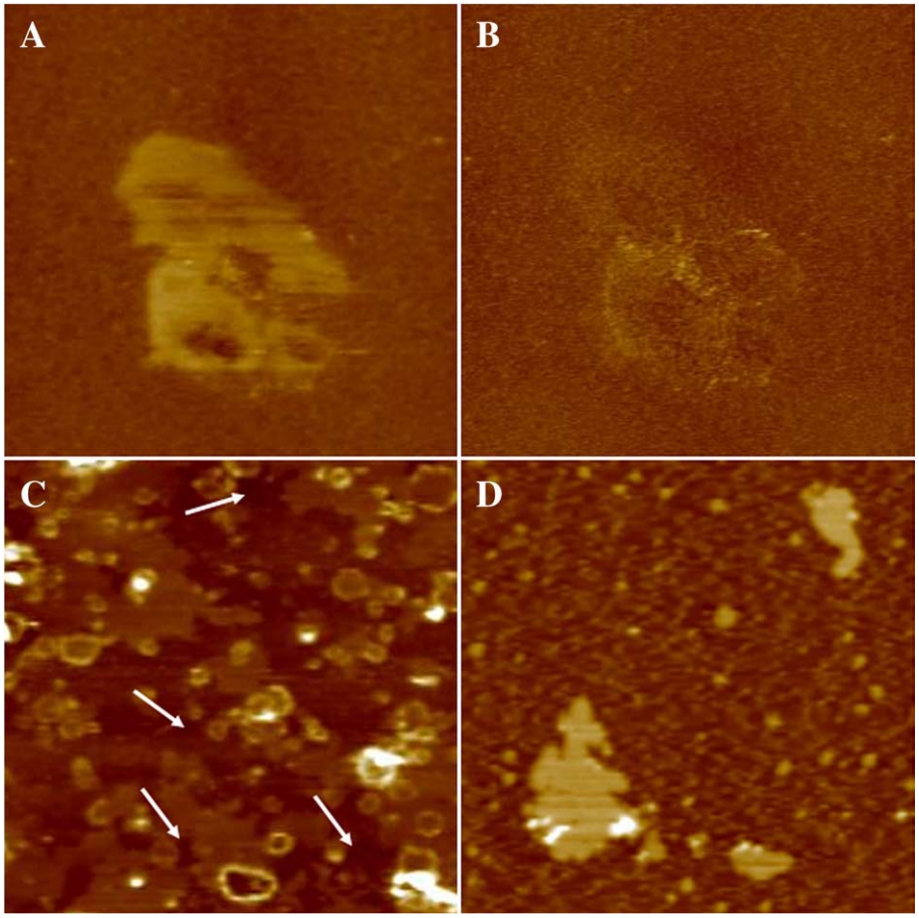

Fig. 6. Contact mode AFM images in liquid (height data) showing the disrupting effect of proteases on DRM lipid domains (A, B): (A) first scan after a 2.0 h sample incubation in the presence of proteases; (B) second scan (about 15 min later); (C) DRMs purified from cells pretreated with Aβ1–42 oligomers. The white arrows indicate some of the cavities resulting from DRM interaction with ADDLs. (D) DRMs purified from cells pretreated with Aβ42–1 oligomers. Scan size 2.5 μm; Z range 10 nm.

mainly at the lipid raft level, or oligomer binding to the membrane itself, in most cases a key step in amyloid cytotoxicity. In PEG-cholesterol supplemented cells, the increase of plasma membrane cholesterol resulted in a reduced ADDL binding to the plasma membrane, as compared to control cells. Conversely, the same oligomers appeared to accumulate mostly at the cell plasma membrane when they were added to the culture medium of cells depleted in membrane cholesterol following treatment with β-CD or Mev. These results suggest that, in our neuronal cell model, the cholesterol content of the cell membrane is inversely correlated with the membrane perturbing effects of Aβ1–42 oligomers. These data agree with our previous findings, which show that neuroblastoma cells enriched in membrane cholesterol display higher resistance to Aβ1–42 oligomer toxicity than untreated or cholesterol-depleted cells [7]. They are also consistent with previous reports showing that disruption of cholesterol homeostasis can be detrimental to cells because toxic Aβ aggregates interact more easily with cholesterol-poor membranes [41,51,59,60]. In particular, our data agree with several reports indicating that the cholesterol content affects membrane physical features such as fluidity and density of lipid packing, hindering both aggregate recruitment at the cell membrane and membrane permeabilization [41]. In particular, the results we obtained in the presence of mevastatin – a specific inhibitor of cholesterol synthesis – support a cholesterol-dependent effect, rather than a generic lipid density-dependent effect at the plasma membrane level.

Previous reports suggest that Aβ binding and aggregation, as detected by ThT or Congo Red staining, occur in lipid raft domains where it is favoured by clusters of the key component GM1 ganglioside [39,61]. It has also been hypothesized that Aβ1–42 adopts an altered conformation upon binding to GM1 and that in such an altered conformation it can act as a seed for Aβ fibrillogenesis in AD brain [61]. Finally, previous findings indicate that GM1 clusters are affected by membrane cholesterol depletion [62]. Actually, our confocal laser microscope analysis showed a marked ADDL-GM1 colocalization on plasma membrane rafts in neuroblastoma cells. Furthermore, in our cell model, cholesterol-depleted lipid rafts displayed enhanced ADDL-GM1 colocalization with respect to control cells, whereas we found a significantly reduced ADDL binding to cholesterol-enriched rafts, as compared to control cells. Our data on ADDL-GM1 colocalization in cholesterol-enriched or -depleted cells agree with previously reported findings on the effect of cholesterol on amyloid aggregate binding to the cell membrane [41,59,60] and suggest that a mild loss of neuronal membrane cholesterol results in an increased binding of ADDLs to neuronal lipid rafts.

There is no consensus on the steady-state fraction of rafts in the cell membranes, their size, location and lipid/protein composition, which might reflect rapid raft dynamics accounting for intrinsic raft heterogeneity in different cultured or tissue cells. There are several procedures described in the literature allowing purification of lipid rafts and caveolae membranes, and the variability of the experimental result can depend on the method used. In this study we choose a widely used method to prepare membrane domains enriched in sphingolipids, monosialogangliosides and cholesterol (DRMs). This experimental approach provides a more appropriate mimic of the lipid rafts found *in vivo* than synthetic raft-like vesicles. However,

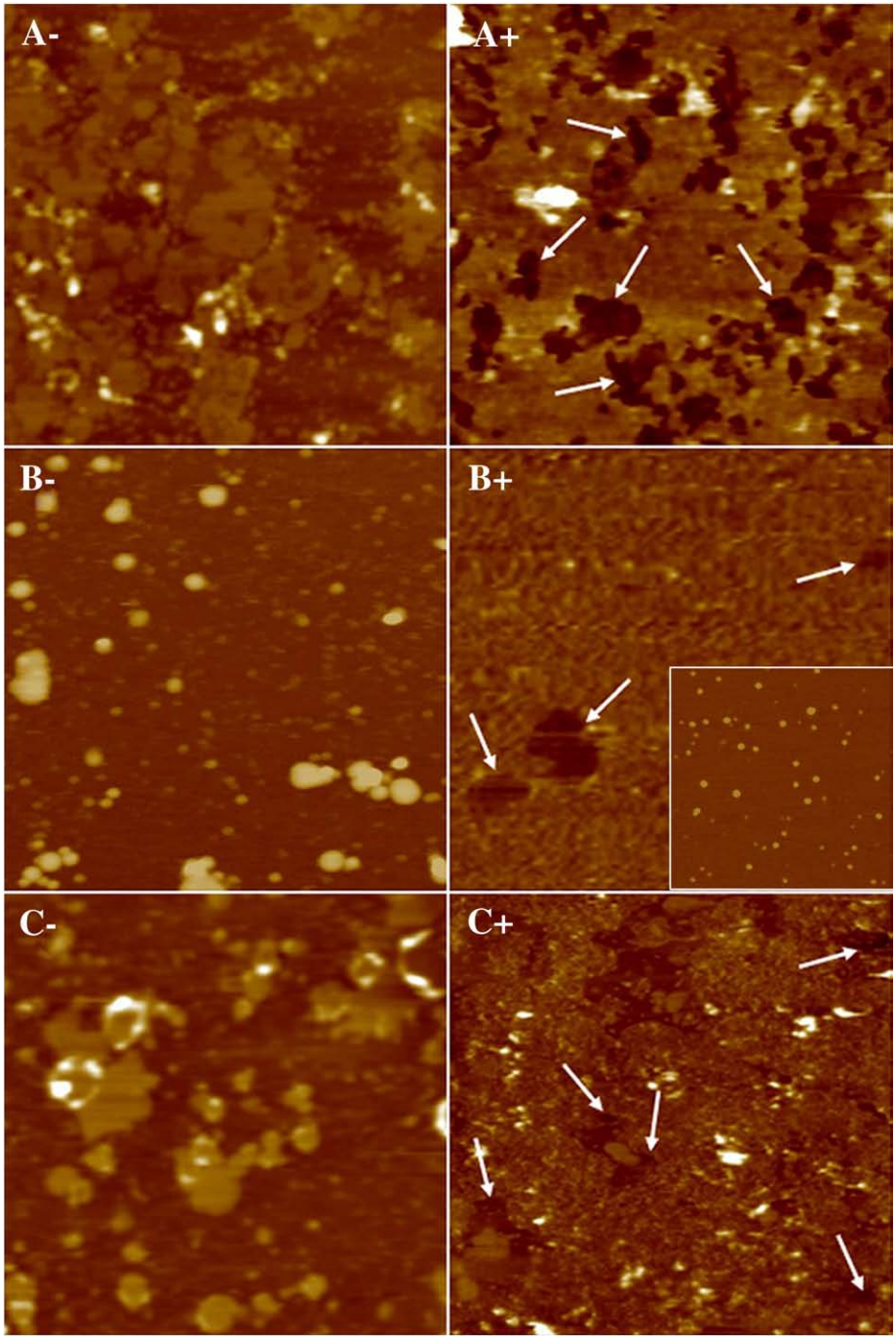

Fig. 7. Contact mode AFM images in liquid (height data) of DRMs before (−) and after (+) 30 min incubation with 1.0 μM Aβ1–42 ADDLs. (A+, A−) DRMs prepared from control cells; (B+, B−) cholesterol-enriched DRMs; (C+, C−) cholesterol-depleted DRMs. The white arrows indicate some of the cavities formed as a consequence of DRM interaction with ADDLs. Scan size 2.5 μm; Z range 10 nm. The inset in (B+) is a tapping mode AFM image of ADDLs. Scan size 1.0 μm; Z range 5.0 nm.

whether, and to what extent, these isolated DRMs reflect the physical, chemical and biochemical organization of lipid rafts *in vivo* remains to be elucidated. Taking into account these caveats, we investigated the ability of ADDLs to interact with purified DRMs and the effect of such interaction on physical and morphological features of the latter.

Our anisotropy fluorescence measurements of sucrose density gradient-purified and flotillin-1-positive DRMs confirmed that there is an inverse relation between cholesterol content and membrane perturbing effects of ADDLs. The DPH probe partitions equally between the ordered and the disordered phases of membrane lipid domains [55]. It is evenly distributed throughout all the lipidic regions in the plasma membrane of a living cell [63,64] and its location is similar in membranes with different content of cholesterol [65]. Therefore, the cholesterol-induced effects on DPH fluorescence polarization here reported reflect differences in DPH motion, rather than in DPH distribution [65]. By using such technique, we found that DRMs microdomains purified from cholesterol-enriched cells are less susceptible to the decrease of fluidity caused by Aβ oligomers as compared to comparable preparations of DRMs purified from control cells. Conversely, the loss of cholesterol resulted in a higher susceptibility of disassembled lipid rafts, not only to Aβ1–42 oligomers but also to the Aβ42–1 monomeric peptide. These results suggest that

the more fluid the lipid raft membrane, the greater its ability to bind non-specifically Aβ1–42 and, possibly, other peptides. We therefore conclude that the presence of β-sheet structure appears to be required for the membrane perturbing properties of Aβ oligomers only in DRMs mimicking raft microdomains with basal cholesterol content, but not in DRMs purified from cholesterol depleted plasma membranes, in agreement with previously reported evidences in synaptosomal plasma membranes [66].

AFM imaging in liquid showed that treatment of DRMs with ADDLs resulted in the formation of large cavities, or hollows. The ADDL–lipid interaction may result in lipid depletion from the bilayer, with the formation of steps reflecting differences between the thickness of a standard bilayer and that of a thinner phase. Similar effects have been observed previously in supported lipid bilayers exposed to prefibrillar amyloid aggregates [56]. A thinner phase may result from lipid interdigitation, as observed in supported lipid bilayers interacting with transmembrane peptides [67]. Alternatively, oligomer interaction with the bilayer may induce *trans–gauche* conformational changes of the lipids, giving rise to a reduced bilayer thickness [68]. The size and depth of the cavities were significantly reduced in DRMs purified from cholesterol-enriched cells, suggesting cholesterol may protect against amyloid-induced cell membrane damage at the lipid raft level. Overall, our results on DRM morphology agree with previous experimental data indicating a protective effect of cholesterol against membrane disassembly by prefibrillar aggregates of proteins and peptides [41]. The formation of cavities was observed also in DRMs purified from cells pre-treated with Aβ1–42 oligomers. However, in this case the depth and size of the cavities were significantly reduced, suggesting that living cells are able to resist, at least in part, ADDL-induced membrane damage.

A typical feature of DRM samples observed by AFM was the presence of domains protruding from the lipid surface. These domains were shown to consist of fluid protein or lipoprotein complexes. In fact, they disappeared in the presence of proteases and displayed higher adhesion forces than the background. We exploited the presence of these fluid domains to characterize the differences between samples with varying cholesterol content and to check the changes induced by their interaction with ADDLs. The domain size increased with decreasing cholesterol content (Table 1), reflecting increased environment fluidity. Actually, increased mobility can favour fluid domain coalescence. On the contrary, domain height decreased with decreasing cholesterol content. The latter finding might be interpreted as the result of an increased compliance of the cholesterol-depleted DRM environment. Treatment of DRMs with ADDLs induced changes in domain morphology that appeared to depend on the content of cholesterol and suggested domain disassembly. In particular, in cholesterol-enriched samples the domain size was almost unaffected by treatment with ADDLs, while in control and cholesterol-depleted samples the domain size after raft treatment with ADDLs was almost half of that measured before treatment.

Domain heights were similar in DRMs purified from control cells and subsequently exposed to ADDLs and in DRMs purified from cells previously exposed to the same Aβ oligomers, suggesting that domain modifications are similar when they occur in the whole intact plasma membrane or in purified membrane fractions. However, pre-treatment with Aβ oligomers did not affect the domain size, which was compatible with that of untreated control cells.

Overall, our data on DRM domains provide information on the structural and morphological features of the cell plasma membrane and its cholesterol- and GM1 ganglioside-enriched raft domains. In particular, we showed that the content of cholesterol affects the ability of ADDLs to interact with the cell membrane by modulating membrane physical features at the raft level. In addition, as far as we know, we imaged for the first time by AFM the morphological features of raft domains purified from the plasma membrane of neurotypic model cells previously enriched or depleted in cholesterol and the different effects on their structure caused by exposure to ADDLs.

Acknowledgements

The authors would like to thank Daniel Wright for critical reading of the manuscript. This study was supported by grants from the Italian MIUR (project number 2007XY59ZJ_001 and 2007XY59ZJ_004), from the Ente Cassa di Risparmio di Firenze and from the University of Genoa (Fondi di Ateneo).

References

[1] D.M. Walsh, I. Klyubin, J.Y. Fadeeva, W.K. Callen, R. Anvyl, M.S. Wolfe, M.J. Rowan, D.J. Selkoe, Naturally secreted oligomers of amyloid β protein potently inhibit hippocampal long-term potentiation in vivo, Nature 416 (2002) 535–539.
[2] J.P. Cleary, D.M. Walsh, J.J. Hofmeister, G.M. Shankar, M.A. Kuskowski, D.J. Selkoe, K.H. Ashe, Natural oligomers of the amyloid-β protein specifically disrupt cognitive function, Nat. Neurosci. 8 (2005) 79–84.
[3] S. Lesné, M.T. Koh, L. Kotlinek, R. Kayed, C.G. Glabe, A. Yang, M. Gallagher, H. Ashe, A specific amyloid-β protein assembly in the brain impairs memory, Nature 440 (2006) 352–357.
[4] D.J. Selkoe, Folding proteins in fatal ways, Nature 426 (2003) 900–904.
[5] D.M. Walsh, D.J. Selkoe, Oligomers on the brain: the emerging role of soluble protein aggregates in neurodegeneration, Protein Peptide Lett. 11 (2004) 1–16.
[6] R. Kayed, E. Head, J.L. Thompson, T.M. McIntire, S.C. Milton, C.W. Cotman, C.G. Glabe, Common structure of soluble amylopid oligomers implies common mechanism of pathogenesis, Science 300 (2003) 486–489.
[7] C. Cecchi, F. Rosati, A. Pensalfini, L. Formigli, D. Nosi, G. Liguri, F. Dichiara, M. Morello, G. Danza, G. Pieraccini, A. Peri, M. Serio, M. Stefani, Seladin-1/dhcr24 protects neuroblastoma cells against abeta toxicity by increasing membrane cholesterol content, J. Cell. Mol. Med. 12 (2008) 1990–2002.
[8] M. Bokvist, F. Lindström, A. Watts, G. Gröbner, Two types of Alzheimer's β-amyloid (1–40) peptide membrane interactions: aggregation preventing transmembrane anchoring versus accelerated surface fibril formation, J. Mol. Biol. 335 (2004) 1039–1049.
[9] A. Deshpande, E. Mina, C. Glabe, J. Busciglio, Different conformations of amyloid beta induce neurotoxicity by distinct mechanisms in human cortical neurons, J. Neurosci. 26 (2006) 6011–6018.
[10] H.R. Bhatia, Lin, R. Lal, Fresh and globular amyloid beta protein (1–42) induces rapid cellular degeneration: evidence for AbetaP channel-mediated cellular toxicity, FASEB J. 14 (2000) 1233–1243.
[11] M. Stefani, C.M. Dobson, Protein aggregation and aggregate toxicity: new insights into protein folding, misfolding diseases and biological evolution, J. Mol. Med. 81 (2003) 678–699.
[12] R. Kayed, Y. Sokolov, B. Edmonds, T.M. McIntire, S.C. Milton, J.E. Hall, C.G. Glabe, Permeabilization of lipid bilayers is a common conformation-dependent activity of soluble amyloid oligomers in protein misfolding diseases, J. Biol. Chem. 279 (2004) 46363–46366.
[13] A. Demuro, E. Mina, R. Kayed, S. Milton, I. Parker, C.G. Glabe, Calcium dysregulation and membrane disruption as a ubiquitous neurotoxic mechanism of soluble amyloid oligomers, J. Biol. Chem. 280 (2005) 17294–17300.
[14] R. Kayed, A. Pensalfini, L. Margol, Y. Sokolov, F. Sarsoza, E. Head, J. Hall, C. Glabe, Annular protofibrils are a structurally and functionally distinct type of amyloid oligomer, J. Biol. Chem. 284 (2009) 4230–4237.
[15] J.A. Allen, R.A. Halverson-Tamboli, M.M. Rasenick, Lipid raft microdomains and neurotransmitter signalling, Nat. Neurosci. 8 (2007) 128–140.
[16] M.J. Morgan, Y.-S. Kim, Z. Liu, Lipid rafts and oxidative stress-induced cell death, Antiox. Redox Signal. 9 (2007) 1471–1483.
[17] A. Kusumi, K. Suzuki, Toward understanding the dynamics of membrane raft-based molecular interactions, Biochim. Biophys. Acta 1746 (2005) 234–251.
[18] A. Crameri, E. Biondi, K. Kuehnle, D. Lütjohann, K.M. Thelen, S. Perga, C.G. Dotti, R.M. Nitsch, M.D. Ledesma, M.H. Mohajeri, The role of seladin-1/DHCR24 in cholesterol biosynthesis, APP processing and Abeta generation in vivo, EMBO J. 25 (2006) 432–443.
[19] C. Hattori, M. Asai, H. Onishi, N. Sasagawa, Y. Hashimoto, T.C. Saido, K. Marayama, S. Mizutani, S. Ishiura, BACE1 interacts with lipid raft proteins, J. Neurosci. Res. 84 (2006) 912–917.
[20] K.S. Vetrivel, H. Cheng, W. Lin, T. Sakurai, T. Li, N. Nukina, P.C. Wong, H. XU, G. Thinakaran, Association of gamma-secretase with lipid rafts in post-Golgi and endosome membranes, J. Biol. Chem. 279 (2004) 44945–44954.
[21] I.S. Yoon, E. Chen, T. Busse, E. Repetto, M.K. Lakshmana, E.H. Koo, D.E. Kang, Low-density lipoprotein receptor-related protein promotes amyloid precursor protein trafficking to lipid rafts in the endocytic pathway, FASEB J. 21 (2007) 2742–2752.
[22] D.R. Taylor, N.M. Hooper, The prion protein and lipid rafts, Mol. Membr. Biol. 23 (2006) 89–99.
[23] S.B. Prusiner, M.R. Scott, S.J. DeArmond, F.E. Cohen, Prion Protein Biology, Cell 93 (1998) 337–348.
[24] D.A. Harris, Cellular biology of prion diseases, Clin. Microbiol. Rev. 12 (1999) 429–444.

[25] D. Sarnataro, V. Campana, S. Paladino, M. Stornaiuolo, L. Nitsch, C. Zurzolo, PrP^c association with lipid rafts in the early secretory pathway stabilizes its cellular conformation, Mol. Biol. Cell. 15 (2004) 4031–4042.
[26] R. Ehehalt, P. Keller, C. Haass, C. Thiele, K. Simons, Amyloidogenic processing of the Alzheimer beta-amyloid precursor protein depends on lipid rafts, J. Cell Biol. 160 (2003) 113–123.
[27] A. Kakio, S. Nishimoto, Y. Kozutsumi, K. Matsuzaki, Formation of a membrane-active form of amyloid beta-protein in raft-like model membranes, Biochem. Biophys. Res. Commun. 303 (2003) 514–518.
[28] T. Suzuki, J. Ito, H. Takagi, F. Saitoh, H. Nawa, H. Shimizu, Biochemical evidence for localization of AMPA-type glutamate receptor subunits in the dendritic raft, Brain Res. Mol. Brain Res. 89 (2001) 20–28.
[29] S. Besshoh, D. Bawa, L. Teves, M.C. Wallace, J.W. Gund, Increased phosphorylation and redistribution of NMDA receptors between synaptic lipid rafts and post-synaptic densities following transient global ischemia in the rat brain, J. Neurochem. 93 (2005) 186–194.
[30] H. Hsieh, J. Boehm, C. Sato, T. Iwatsubo, T. Tomita, S. Sisodia, R. Malinow, AMPAR removal underlies Aβ-induced synaptic depression and dendritic spine loss, Neuron. 52 (2006) 831–843.
[31] F.G. De Felice, P.T. Velasco, M.P. Lambert, K. Viola, S.J. Fernandez, S.T. Ferreira, W.L. Klein, Aβ oligomers induce neuronal oxidative stress through an N-methyl-D-aspartate receptor-dependent mechanism that is blocked by the Alzheimer drug memantine, J. Biol. Chem. 282 (2007) 11590–11601.
[32] Y. Wu, A.C. Aral, G. Rumbaugh, A.K. Srivastava, G. Turner, T. Hayashi, E. Suzuki, Y. Jiang, L. Zhang, J. Rodriguez, J. Boyle, P. Tarpey, F.L. Raymond, J. Nevelsteen, G. Froyen, M. Stratton, A. Futreal, J. Gecz, R. Stevenson, C.E. Schwartz, D. Valle, R.L. Huganir, T. Wang, Mutations in ionotropic AMPA receptor 3 alter channel properties and are associated with moderate cognitive impairment in humans, Proc. Natl. Acad. Sci. U. S. A. 104 (2007) 18163–18168.
[33] S.I. Kim, J.S. Yi, Y.G. Ko, Amyloid beta oligomerization is induced by brain lipid rafts, J. Cell. Biochem. 99 (2006) 1878–1889.
[34] J.M. Cordy, I. Hussain, C. Dingwall, N.M. Hooper, A.J. Turner, Exclusively targeting beta-secretase to lipid rafts by GPI-anchor addition up-regulates beta-site processing of the amyloid precursor protein, Proc. Natl. Acad. Sci. U. S. A. 100 (2003) 11540–11573.
[35] R. Ehehalt, P. Keller, C. Haass, C. Thiele, K. Simons, Amyloidogenic processing of the Alzheimer beta-amyloid precursor protein depends on lipid rafts, J. Cell Biol. 160 (2003) 113–123.
[36] M. Morishima-Kawashima, Y. Ihara, The presence of amyloid beta protein in the detergent-insoluble membrane compartment of human neuroblastoma cells, Biochemistry 37 (1998) 15247–15253.
[37] L. Saavedra, A. Mohamed, V. Ma, S. Kar, E. Posese de Chaves, Internalization of β-amyloid peptide by primary neurons in the absence of apolipoprotein, J. Biol. Chem. 282 (2007) 35722–35732.
[38] T.Y. Chen, P.H. Liu, C.T. Ruan, L. Chiu, F.L. Kung, The intracellular domain of amyloid precursor protein interacts with flotilin-1, a lipid raft protein, Biochem. Biophys. Res. Commun. 342 (2006) 266–272.
[39] R. Williamson, A. Usardi, D.P. Hanger, B.H. Anderton, Membrane-bound β-amyloid oligomers are recruited into lipid rafts by a Fyn-dependent mechanism, FASEB J. 22 (2008) 1552–1559.
[40] M.D. Ledesma, C.G. Dotti, The conflicting role of brain cholesterol in Alzheimer's disease: lessons from the brain plasminogen system, Biochem. Soc. Symp. 72 (2005) 129–138.
[41] N. Arispe, M. Doh, Plasma membrane cholesterol controls the cytotoxicity of Alzheimer's disease Abeta(1–40) and (1–42) peptides, FASEB J. 16 (2002) 1526–1536.
[42] M.P. Lambert, K.L. Viola, B.A. Chromy, L. Chang, T.E. Morgan, J. Yu, D.L. Venton, G.A. Krafft, C.E. Finch, W.L. Klein, Vaccination with soluble Aβ oligomers generates toxicity-neutralizing antibodies, J. Neurochem. 79 (2001) 595–605.
[43] D.M. Amundson, M. Zhou, Fluorometric method for the enzymatic determination of cholesterol, J. Biochem. Biophys. Methods 38 (1999) 43–52.
[44] J.G. Mohanty, J.S. Jaffe, E.S. Schulman, D.G. Raible, A highly sensitive fluorescent micro-assay of H_2O_2 release from activated human leukocytes using a dihydroxyphenoxazine derivative, J. Immunol. Methods 202 (1997) 133–141.
[45] M.R. Hojjati, X. Jiang, Rapid, specific, and sensitive measurements of plasma sphingomyelin and phosphatidylcholine, J. Lipid. Res. 47 (2006) 673–676.
[46] A. Relini, O. Cavalleri, C. Canale, T. Svaldo-Lanero, R. Rolandi, A. Gliozzi, What can atomic force microscopy say about amyloid aggregates? in: B. Bushan, H. Fuchs, M. Tomitori (Eds.), Applied Scanning Probe Methods IX – Characterization, Springer Verlag, Heidelberg, 2008, pp. 177–206, cap. 20.
[47] O. Simakova, N.J. Arispe, The cell-selective neurotoxicity of the Alzheimer's Abeta peptide is determined by surface phosphatidylserine and cytosolic ATP levels. Membrane binding is required for Abeta toxicity, J. Neurosci. 27 (2007) 13719–13729.
[48] W.S. Rasband, ImageJ, U. S. National Institutes of Health, Bethesda, Maryland, USA, 1997-2008, http://rsb.info.nih.gov/ij/.
[49] M.M. Bradford, A rapid sensitive method for the quantitation of microgram quantities of protein utilizing the principle of protein-dye binding, Anal. Biochem. 72 (1976) 248–254.
[50] E. Romiti, E. Meacci, G. Tanzi, L. Becciolini, S. Mitsutake, M. Farnararo, M. Ito, P. Bruni, Localization of neutral ceramidase in caveolin-enriched light membranes of murine endothelial cells, FEBS Lett. 506 (2001) 163–168.
[51] C. Cecchi, S. Baglioni, C. Fiorillo, A. Pensalfini, G. Liguri, D. Nosi, S. Rigacci, M. Bucciantini, M. Stefani, Insights into the molecular basis of the differing susceptibility of varying cell types to the toxicity of amyloid aggregates, J. Cell Sci. 118 (2005) 3459–3470.
[52] C. Cecchi, A. Pensalfini, M. Stefani, S. Baglioni, C. Fiorillo, S. Cappadona, R. Caporale, D. Nosi, M. Ruggiero, G. Liguri, Replicating neuroblastoma cells in different cell cycle phases display different vulnerability to amyloid toxicity, J. Mol. Med. 86 (2008) 197–209.
[53] W.G. Wood, F. Schroeder, N.A. Avdulov, S.V. Chochina, U. Igbavboa, Recent advances in brain cholesterol dynamics: transport, domains and Alzheimer's disease, Lipids 34 (1999) 225–234.
[54] M. Shinitzky, Y. Barenholz, Dynamics of the hydrocarbon layer in liposomes of lecithin and sphingomyelin containing dicetylphosphate, J. Biol. Chem. 249 (1974) 2652–2657.
[55] B.R. Lentz, Membrane "fluidity" as detected by diphenylhexatriene probes, Chem. Phys. Lipids 50 (1989) 171–190.
[56] C. Canale, S. Torrassa, P. Rispoli, A. Relini, R. Rolandi, M. Bucciantini, M. Stefani, A. Gliozzi, Natively folded HypF-N and its early amyloid aggregates interact with phospholipid monolayers and destabilize supported phospholipid bilayers, Biophys. J. 91 (2006) 4575–4588.
[57] H. Egawa, K. Furusawa, Liposome adhesion on mica surface studied by atomic force microscopy, Langmuir 15 (1999) 1660–1666.
[58] Z. Leonenko, E. Finot, D. Cramb, AFM study of interaction forces in supported planar DPPC bilayers in the presence of general anesthetic halothane, Biochim. Biophys. Acta 1758 (2006) 487–492.
[59] C.M. Yip, E.A. Elton, A.A. Darabie, M.R. Morrison, J. McLaurin, Cholesterol, a modulator of membrane-associated Abeta-fibrillogenesis and neurotoxicity, J. Mol. Biol. 311 (2001) 723–734.
[60] M. Kawahara, Y. Kuroda, N. Arispe, E. Rojas, Alzheimer's beta-amyloid, human islet amylin, and prion protein fragment evoke intracellular free calcium elevations by a common mechanism in a hypothalamic GnRH neuronal cell line, J. Biol. Chem. 275 (2000) 14077–14083.
[61] K. Yanagisawa, Role of gangliosides in Alzheimer's disease, Biochim. Biophys. Acta 1768 (2007) 1943–1951.
[62] A. Fujita, J. Cheng, M. Hirakawa, K. Furukawa, S. Kusunoki, T. Fujimoto, Gangliosides GM1 and GM3 in the living cell membrane form clusters susceptible to cholesterol depletion and chilling, Mol. Biol. Cell. 18 (2007) 2112–2122.
[63] B.R. Lentz, Use of fluorescent probes to monitor molecular order and motions within liposome bilayers, Chem. Phys. Lipids 64 (1993) 99–116.
[64] M. Companyó, A. Iborra, J. Villaverde, P. Martínez, A. Morros, Membrane fluidity changes in goat sperm induced by cholesterol depletion using beta-cyclodextrin, Biochim. Biophys. Acta 1768 (2007) 2246–2255.
[65] R.D. Kaiser, E. London, Location of diphenylhexatriene (DPH) and its derivatives within membranes: comparison of different fluorescence quenching analyses of membrane depth, Biochemistry 37 (1998) 8180–8190.
[66] G.P. Eckert, W.G. Wood, W.E. Müller, Membrane disordering effects of beta-amyloid peptides, Subcell Biochem. 38 (2005) 319–337.
[67] H.A. Rinia, R.A. Kik, R.A. Demel, M.M.E. Snel, J.A. Killian, J.P.J.M. van der Eerden, B. de Kruijff, Visualization of highly ordered striated domains induced by transmembrane peptides in supported phosphatidylcholine bilayers, Biochemistry 39 (2000) 5852–5858.
[68] H.W. Teller, A.J. Waring, R.I. Lehrer, T.A. Harroun, T.M. Weiss, L. Yang, H.W. Huang, Membrane thinning effect of the β-sheet antimicrobial peptide protegrin, Biochemistry 39 (2000) 139–145.